M. Boada, A. Lázaro, R. Villarino and D. Girbau. “Battery-Less Moisture Measurement System Based on a NFC Device with Energy Harvesting Capability”, IEEE Sensors Journal, vol. 18(13), pp. 5541-5549, May 2018.

doi: 10.1109/jsen.2018.2837388

URL: https://ieeexplore.ieee.org/document/8360092

Battery-Less Soil Moisture Measurement System Based on a NFC Device with Energy Harvesting Capability

Martí Boada, Antonio Lazaro, *Senior Member, IEEE*, Ramon Villarino, David Girbau, *Senior Member, IEEE*
Departament d'Enginyeria Electrònica, Elèctrica i Automàtica (DEEEA)
Universitat Rovira i Virgili (URV), 43007 Tarragona, Spain

***Abstract*—A novel moisture sensor based on Near Field Communication (NFC) is presented. The system consists of a battery-less sensing device which measures temperature, relative humidity and the volumetric water content, and is powered from the magnetic field generated by the reader. In order to compute the sensed data, the system includes a microcontroller, which has been programmed to make the calculations and to send the processed data to the NFC chip through an I^2C bus. This data is stored into the EEPROM memory of the NFC integrated circuit in NFC Data Exchange Format (NDEF), which is read by the reader. An analysis of different methods to measure the soil moisture is presented in order to select the approach which fits better with the constraints of a NFC energy harvested system.**

Index Terms—Battery-less, Energy Harvesting, NFC, Relative Humidity, Sensor, Soil moisture, Temperature, Volumetric Water Content

I. Introduction

NEAR FIELD COMMUNICATION (NFC) is a Radiofrequency IDentification system (RFID) that allows fast communication between devices in a short range. Although near-field communications exist from more than a decade [1], this technology has not been extended until the massive use in payment systems. Furthermore, currently most smartphones incorporate an NFC reader. Thus, the importance of NFC systems within the Internet of Things (IoT) scenario is growing. NFC is also interesting for the development of low-cost sensors, since it provides a fast and easy way to get the data from them, simply approaching the reader to the tag, without need of pairing the devices. Moreover, NFC manufacturers such as AMS [2], NXP [3] or ST Microelectronics [4] offer to the market advanced integrated circuits (IC) with energy harvesting capabilities. These chips take part of the energy received by the magnetic field generated at the reader to provide an analog voltage output that can be used to power external electronics such as low-power microcontrollers or sensors. Due to the short range of such systems, the amount of power that can be harvested is considerably larger than that available in far-field RFID systems. The progressive introduction into the market of these ICs allows for the development of low-cost battery-less portable sensors such as skin temperature sensors [5] or pH sensors to monitor wounds healing [6].

Soil moisture measurement is a key aid for irrigation water management. Regulating irrigation is crucial to satisfy the water requirement of crops without wasting water, to treat the soil correctly, and to control the plant nutrients in order to save energy. Most sophisticated systems are automated using climate-based electronic controllers whereas the simplest ones repeat a set of scheduled tasks as function of time. Low-cost monitoring systems are demanded for personal use at home or to monitor a particular crop, as for example in a greenhouse or plants shop. In these cases, irrigation is often manual or semiautomatic and the conditions are usually specific for each crop. Therefore, the control of the soil moisture must be taken into account for an appropriated plant care. There are several soil moisture measurement techniques [7] but most of them are not suitable for amateur or low-cost applications. Most typical portable low-cost meters use a sensor connected to the analog-to-digital converter (ADC) of a microcontroller, which translates a physical value to the corresponding magnitude. The result is often shown in a display or acquired by an external data logger. In all the cases these methods use a battery to supply energy to the electronic components.

Several wireless soil moisture sensors can be found on the literature [8][9]. However, those sensors require an expensive reader (in the case of RFID systems), or batteries and expensive chips in the case of Bluetooth. NFC has as an advantage in its price (less than 1 euro per NFC IC), and the possibility to use any conventional smartphone as reader, which can upload the sensed data to the cloud. The limitation is in the readout range (few centimeters), a characteristic that defines a frame of applications and usages where NFC is very attractive and also define the areas where this technology is restricted.

This work proposes a soil moisture sensor embedded in a passive NFC-based tag, which powers up the electronics harvesting the energy provided by the reader. The data obtained can be stored into an Internet of Things (IoT) database to be used to program the irrigation schedule and to keep track of the soil conditions. On the other hand, no additional cost for the reader is required since it is a commercial. The tag also integrates ambient temperature and humidity sensors to

Manuscript received Jan. 5, 2018. This work was supported by the Spanish Government Project TEC2015-67883-R, BES-2016-077291 and H2020 Grant Agreement 645771–EMERGENT. M.Boada, A.Lazaro, R.Villarino, D.Girbau are with the Department of Electronic, Electric and Automatic Control Engineering, Universitat Rovira i Virgili, 43007 Tarragona, Spain (e-mail: antonioramon.lazaro@urv.cat).

complement the information of the environment since these parameters may affect the irrigation schedule. The tags can be installed in several points for individual monitoring thanks to its low cost. In addition to the sensed data, an identification tag number is written into the NFC chip which can be related to information about the plant (name, origin, brief description, specific cares) which can be retrieved by the reader and displayed in a custom app.

The paper is organized as follows. Section II provides a review of available soil measurement systems in the literature. From this review a justification of a capacitive soil measurement technique for the proposed application is given. Section III describes the system. Section IV presents some measurements and a method to calibrate the sensor. Finally, Section V gives some conclusions.

II. Soil Moisture Measurement Techniques

The soil moisture content is often expressed as the Volumetric Water Content (VWC), defined as the volume of water over the total volume, as it is shown in the example of Fig. 1.

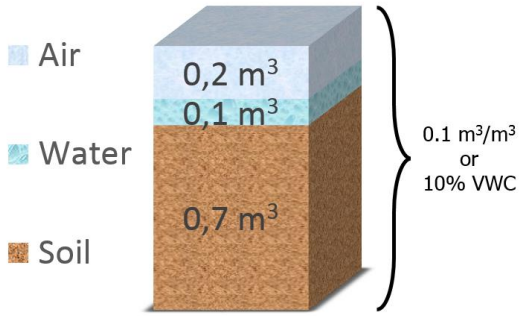

Fig. 1. Representation of 1 m^3 separated into constituent parts where 70% of the total volume is the soil, 10% is water and 20% is air.

Within the bunch of existing techniques to measure soil moisture content there are direct and indirect methods. The most known direct method is the thermo-gravimetric [7], which is usually used as a standard reference. However, it requires at least one day to get the result and it cannot be performed *in situ*. This method is therefore used for calibration of other sensors in laboratories. On the other hand, there are several indirect techniques [10]. The most common ones are listed below.

Neutron Moisture Meters (NMM) have a large action radius and are insensitive to temperature and salinity. However, it is an expensive method which requires a certification for radiation [11]. Therefore, it can be used on research but it is not suitable for personal use.

Thermal sensors take advantage of the difference of heat conductance between soil and water. They measure the change on temperature of the surround soil after applying a heat pulse [12]. This type of sensors are inexpensive and easy to use but they are very dependent on the soil temperature, they present a long integration time and they are fragile since the distance between the heater and the thermocouple must be kept.

Electrical resistance blocks or gypsum blocks [13] are made with gypsum around a pair of stainless steel wires. Most of the probes are based on the measurement of their electrical resistance. Portable probes are available and can be placed in the soil to give the water proportion reading. The main limitation of this approach is the calibration of the probe due to the potential corrosion of the wires with the accumulation of mineral salts.

Besides the above techniques, there are other methods which make use of the dielectric property of the soil to measure its moisture content. These methods are based on the huge difference of the dielectric constant of dry soil (between 3 and 7), and pure water (about 80). Within these dielectric techniques, Time Domain Reflectometry (TDR) is one of the most common [14][15]. It consists of sending electromagnetic pulses along two wave guides of a well-known length, and measuring the time delay between the incident and reflected waves. The time delay changes according to the dielectric constant of the soil where they are sunk. However, TDR systems are expensive for domestic applications or when several measuring points need to be monitored, which requires multiplexers to share the readout unit [16].

Still within the dielectric techniques, there are the Frequency Domain Reflectometry (FDR) [17] and capacitive techniques [18], both based on the same working principle. In the case of FDR, the dielectric constant of the soil is determined by applying an oscillating charge to the circuit and measuring its resonant frequency to detect variations on the soil's capacitance [19][20]. The main drawback of this technique is that measuring the resonant frequency requires expensive impedance meters. On the other hand, capacitive methods measure directly the capacitance, usually from the charge time of the capacitor. Since these type of sensors are AC excited and the probe can be covered by a protective layer [21], they are not affected by corrosion. Nonetheless, capacitive measurements often require additional signal conditioning for the measurement with a microcontroller, whereas resistive sensors do not.

Despite the foregoing, a capacitive sensor is the one which better fits with the NFC scenario because printed capacitive sensors for soil measurements are compatible with standard PCB technology used for the design of the coil and integrate the electronics of the NFC sensor. In addition, it is not affected by corrosion issues. A critical point for using this kind of sensor is finding a precise capacitance measurement method compatible with the power available from the RF harvesting, an issue addressed in the next section. In this work, a low-power capacitive soil sensor will be developed integrated within a NFC tag and it is described in section III.

III. System Design

A. System Overview

Fig. 2 depicts the system proposed in this work. It is composed by an NFC antenna which is connected to the NFC/RFID IC M24LR04E-R [2], from ST Microelectronics, responsible of receiving and sending NFC Data Exchange Format (NDEF) messages. This device presents the specifications required for this work such as I^2C interface, energy harvesting with 4 configurable currents, and ISO 15693 compatibility. When a magnetic field from a reader is received by the antenna, the NFC IC wakes up automatically. If the energy harvesting mode is activated and the strength of the

magnetic field is enough (higher than a threshold that depends on the energy harvesting configuration of the chip) the M24LR04E-R gets the excess of energy received from the RF field to feed all the components of the system. This chip is capable to provide currents up to 6 mA in the highest current sink mode.

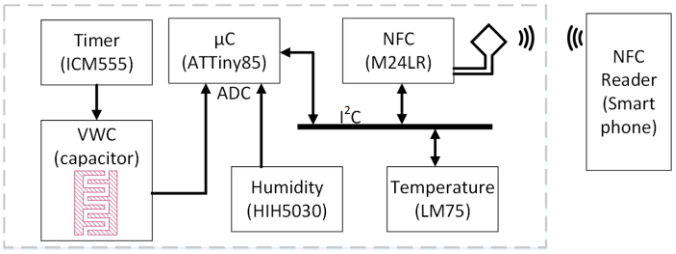

Fig. 2. System overview.

The antenna is a square loop of 50 mm × 50 mm printed on FR4 PCB. There is a total of 6 loops whose width is 0.6 mm. It is designed with Keysight Momentum electromagnetic simulator. The measured inductance is 3.2 µH in agreement with the simulations. A tuning capacitance of 15 pF is added to the internal capacitance of the IC (27.5 pF) to adjust the resonance at 13.56 MHz.

A low-power Atmel 8-bit AVR ATtiny85 microcontroller [20] has been selected to be integrated in the prototype. It can be configured at different clock speeds and can work down to 1.8V, reducing the clock frequency. Due to the power limitations presented by this system, it has been configured to work at 1 MHz, being its consumption around 300 µA at 3.3V. In addition, it can be programmed with Arduino IDE, which is very popular in open-hardware implementations. This microcontroller has an I²C interface and 2 analog inputs. In order to provide more information to the user, the system also includes a humidity sensor, which is connected to an analog input of the microcontroller, and a temperature sensor, which is used to adjust the moisture sensor curve. The temperature sensor is a low-cost I²C sensor LM75A [23], which consumes less than 280 µA in active mode and 4 µA in sleep mode (at 3V). It is an industry-standard digital temperature sensor with an integrated sigma-delta 9-bit resolution ADC, enough for the proposed application. The temperature accuracy is about 1 ºC from -25ºC to 100ºC. The HIH-5030 is a low-voltage humidity sensor that operates down to 2.7 V, with a typical current consumption of only 200 µA [24]. This humidity sensor presents a linear output voltage related to the relative humidity. However, an improved readout can be used if the temperature is known.

TABLE I
CURRENT CONSUMPTION

Element	Consumption (µA)
NFC (M24LR)	400
µC (ATtiny85)	300
Humidity (HIH5030)	200
Temperature (LM75)	280
Timer (ICM555)	60

The technique used for the measurement of soil water content, as it is described below, uses an ICM555 timer oscillator, which is a low-voltage and low-power version of the popular 555 timer, which consumes typical currents of 60 µA at 3V and yields a stable frequency output.

Table I summarizes the current consumption of the different electronic modules integrated in the tag. The energy harvesting needed is in the order of 1 mA at 3 V to power the overall system.

B. Volumetric Water Content measurement

Following the discussion of Section II, there are several methods to measure the Volumetric Water Content of the soil. The approach presented in this work is based on an interdigital capacitor which is sunk in the soil. The dielectric permittivity of the soil depends largely on the changes of the water volume content. Keeping the strip-lines of the interdigital capacitor in contact with the soil allows to measure the dielectric permittivity changes, and then retrieve the soil's VWC.

1) Capacitor

The capacitive sensor is implemented using an interdigital capacitor (IDC) without ground plane (see Fig. 3). Although various technologies can be used to realize these type of sensors, printed circuit board technology is particularly advantageous. The prototype of capacitive sensor has been fabricated using standard Fiber-Glass substrate (FR4) with 34 µm of copper metallization. An insulator layer is added to prevent that electrodes can be shorted in presence of water. Solder mask coating or a thin protection layer of plastic (this latter in the prototypes) can be used as insulator. Fig. 3 shows the shape of an interdigital capacitor indicating the different parameters that influence on its capacitance, which depends on length *L*, gap distance between two conductors *g*, finger width *s*, as well as the number of fingers *N*.

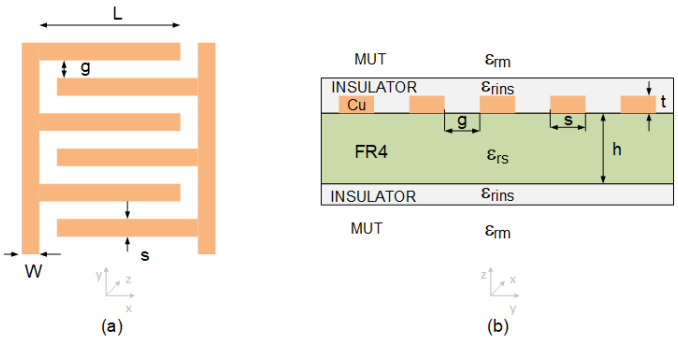

Fig. 3. (a) Top view of an interdigital capacitor. (b) Cross section view of the interdigital capacitor.

Closed-form expressions for multilayer interdigital capacitors have been proposed in the literature [25]. The capacitance can be expressed as the sum of three contributions:

$$C = C_3 + C_n + C_{end} \quad (1)$$

Where C_3, C_n, and C_{end} represent the three-finger capacitance, the capacitance of the periodical (N-3) structure, and a correction term for the fringing fields of the ends of the strips, respectively. These capacitances are proportional to the effective permittivity and the geometrical factors a_3, a_n and a_{end},

that are function of the elliptic integrals of the fist kind *K(k)* resulting of the conforming mapping method [25]:

$$C_3 = \varepsilon_{re3} a_3 L \quad (2)$$

$$C_n = \varepsilon_{rn} a_n (N-3) L \quad (3)$$

$$C_{end} = \varepsilon_{re,end} a_{end} \quad (4)$$

The effective relative permittivity ($\varepsilon_{re,i}$ with i=3, n, end) can be calculated from the filling factor (q_i) that is the percentage of fields in each material for each case:

$$\varepsilon_{rei} = \varepsilon_{rm} + q_{1i}\frac{\varepsilon_{rins}-\varepsilon_{rm}}{2} + q_{2i}\frac{\varepsilon_{rS}-\varepsilon_{rins}}{2} + q_{3i}\frac{\varepsilon_{rins}-\varepsilon_{rm}}{2} \quad (5)$$

Where ε_{rm} and ε_{rs} are the relative permittivity of the medium when the IDC is immersed and of the PCB substrate, respectively. Whereas ε_{rins} is the permittivity of the insulator layer.

For long fingers (L>>s) the correction for fringing fields at the ends of the fingers can be neglected [25]. Therefore, the capacitance *C* is mainly proportional to the length and the number of fingers (N). Replacing (2-4) into (1) the linear expression (6) for the capacity *C* as a function of the medium permittivity expression for the IDC capacitance can be found.

$$C = A + B\varepsilon_{rm} \quad (6)$$

Where *B* depends on the geometry, and *A* depends on the dielectric permittivity of the PCB substrate and insulator. The values *A* or *B* can be obtained using closed-form formulas [21] or by simulation using a full-wave simulator.

In this work the electromagnetic simulator Keysight-Momentum is used for the IDC design and evaluation. In order to obtain a value of capacitance easily readable compatible with the minimum gap and trace width achievable with the available PCB fabrication technology. An IDC with N=40, L=30 mm, W=0.8 mm, s=0.8 mm, g=0.5 mm, h=0.8 mm, t=34 µm, ε_{rs}=4.7 has been designed. Two prototypes with two insulator materials and thickness have been manufactured. The first prototype uses an insulator (type 1) that consist of a coating of adhesive plastic (εrins=2) and with a thickness of 100 µm. In the second prototype, the insulator (type 2) is an acrylic coating spray (εrins=2.7) with a thickness of about 15 µm.

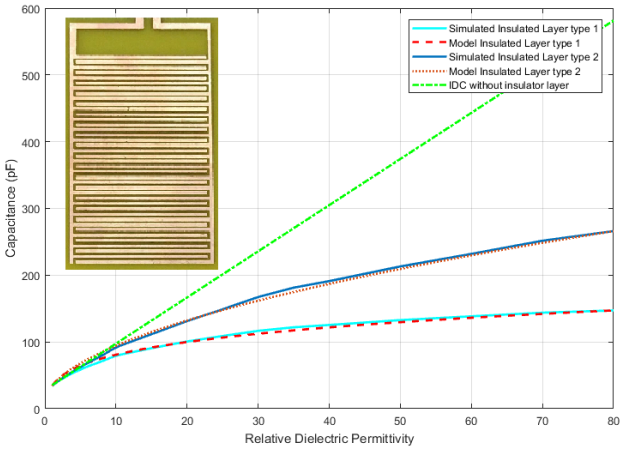

Fig. 4. Simulated and modelled capacitance as a function of the relative dielectric permittivity. Insulator layer type 1 is an adhesive plastic, and type 2 is acrylic coating spray. A photograph of the manufactured IDC is also shown in the inset figure.

Fig. 4 shows a simulation of the IDC capacitance as a function of the relative permittivity of the immersed material under test (MUT). The thickness of MUT is assumed infinite. A linear dependence is observed when an ideal IDC without insulator layer is analyzed. However, the insulator layer introduces a reduction on the sensitivity of the IDC as a function of the permittivity for values of relative dielectric permittivity higher than 10. In addition, the sensitivity (slope as a function of relative permittivity) is not constant as predicted by the closed-form expressions derived from the partial capacitance method [25]. The smaller capacitance values obtained compared with the case without insulator are explained because the effective permittivity of the insulator layer and MUT is smaller than ε_{rm}. The relation between the effective permittivity and the permittivities of the insulator layer and MUT is not linear like in multilayer microstrip lines [26].

Figure 5 shows a cross-section view of the IDC sensor with the equivalent circuit for low permittivity of the MUT (Fig.5.a) and for high permittivities (Fig.5b). In the first equivalent circuit, the capacitance due to the insulator layer (C_{INS}) is in parallel with the capacitance due to the MUT (C_{MUT}), whereas in the second, C_{INS} is in series with C_{MUT}. The first equivalent circuit is used in the derivation of closed formulas from [25]. In the second circuit, when analyzing the fringing electric field path from one electrode to another electrode, it makes more sense that both the capacitance of the insulation layer C_{INS} and the capacitance of MUT C_{MUT} must be connected in series for high dielectric constant values of the MUT [27]. Therefore, it is expected that the effective permittivity and capacitance will be smaller in the second equivalent circuit. Simulated values of C on Fig. 4 agree with the measured capacitance when the IDC is on air (being air the insulator layer, with ε_{rm} =1), 23 pF. C also agrees when the IDC is immersed in water ($\varepsilon_{rm}\approx$80), C=140 pF, for the first prototype (insulator type 1) and 270 pF for the insulator type 2. In order to interpolate the values of capacitance, a compact expression is proposed:

$$C = C_1 + (C_2 - C_1)\frac{(\epsilon_{rm})^{\gamma}-(\epsilon_{rm1})^{\gamma}}{(\epsilon_{rm2})^{\gamma}-(\epsilon_{rm1})^{\gamma}} \quad (7)$$

Where C_1 and C_2 are the capacitance for two known permittivities, ε_{rm1}=1 (air case) and ε_{rm2}=80 (water case), respectively. The exponent γ is a fitting parameter. A value of γ=0.21 is obtained for the IDC of Fig. 4.

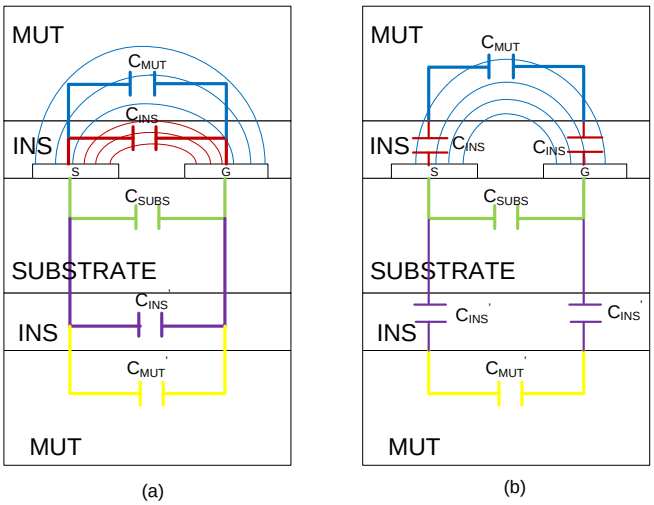

Fig. 5. (a) Cross-section view of IDC sensor with its superimposed equivalent circuit. For low permittivity of MUT used in partial capacitance technique [25] and (b) proposed equivalent circuit for high permittivity of MUT [27].

2) Capacitance measurement

The reduction of clock frequency of the microcontroller to reduce its power consumption introduces some restrictions. In order to decrease the number of components of the tag and reduce, consequently, its cost, the microcontroller clock frequency is fixed using its own internal oscillator. Thus the precision on capacitance measurement based on the discharge time of the capacitor is not enough for small capacitances, since when it is in the order of pF, large time constants must be considered. Taking into account that when near field communication is used the power is only available when the reader is close to the tag, a fast measurement method must be applied. A similar problem arises when an oscillator whose frequency depends on the capacitance is used. In this method, the microcontroller works as a frequency counter and the precision depends on the maximum clock frequency. The methodology used in this paper to measure the capacitance is shown in Fig. 5. A custom frequency-to-voltage converter has been designed because the available commercial IC converters require higher currents than the ones available in this system. A low-power timer is used to generate an AC signal, which is filtered by a low-pass filter (RC filter), whose cut off frequency depends on the capacitance under test. The AC amplitude at the output of the filter is measured using a half-wave rectifier used as detector. The DC voltage filtered at the output of the detector is measured with the internal analog-to-digital converter of the microcontroller. Although the output voltage depends on the power supply, thanks to the fact that the microcontroller uses that voltage as a reference, this problem is avoided.

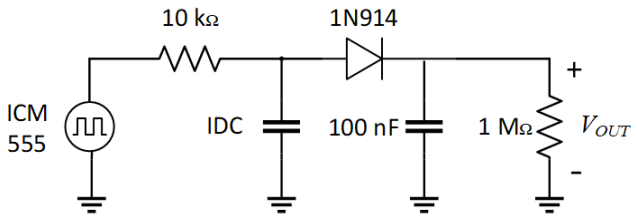

Fig. 6. Circuit to obtain a voltage proportional the interdigital capacitor (IDC) value.

The proposed solution consists of feeding the circuit with a square wave of 380 kHz into a low-pass filter consisting of a resistor of 10 kΩ (R_1) and the interdigital capacitor (IDC), whose value varies in the range 55-270 pF. The resulting signal ($V_{det,}$ which presents a triangular waveform) is rectified by a diode (D). The cathode of the diode is connected to a capacitor (100 nF, C_1) and a shunt resistor (1 MΩ, R_2). Hence at the output of the envelope detector V_{OUT} is proportional to the value of the IDC.

The waveform at the output of the 555 timer is a square wave with nearly ideal 50% duty cycle. This periodic signal can be expanded using Fourier series. The higher harmonics are filtered, therefore only the first harmonic is considered. Then the input signal at the filter can be expressed as:

$$V_{in}(t) = \frac{V_{cc}}{2} + \frac{V_{cc}}{\pi}\cos(\omega t) \qquad (8)$$

Considering $H(j\omega)$ as the transfer function of the low-pass filter defined as:

$$H(j\omega) = \frac{V_{det}}{V_{in}} = \frac{1}{1+j\omega RC} \qquad (9)$$

The voltage at its output is given by:

$$V_{det}(t) = \frac{V_{cc}}{2} + \frac{V_{cc}}{\pi}|H(j\omega)|\cos(\omega t + \varphi) \qquad (10)$$

Where φ is the phase of the transfer function. Therefore, the output of the half-wave detector is proportional to the average amplitude:

$$V_{OUT} = \frac{V_{cc}}{2} - V_f + k|H(j\omega)|V_{cc} \approx \frac{V_{cc}}{2} - V_f + \frac{kV_{cc}}{\omega R}\frac{1}{C} \qquad (11)$$

Where k is a factor that depends on the waveform at the output of the filter (nearly triangular), V_{cc} is the supply voltage, and V_f is an offset correction that takes into account the forward voltage of the diode. If the frequency of the oscillator is chosen higher than the cut-off frequency of the filter f>>1/(2πRC), the signal at the output of the detector is approximately proportional to the inverse of the capacitance. Fig. 6 compares the model given by (5), the circuit simulations considering a conventional silicon diode (1N914), the measurements with a multimeter, and the measures read by the NFC reader. Assuming a nearly triangular waveform at the filter's output, the value of k is 0.5. The forward correction is obtained empirically and it is considered V_f=0.35V. Good agreement has been obtained. Different values of 0603 Surface Mount (SMD) capacitors have been mounted to emulate the IDC and the measurements have been performed both using a multimeter (Agilent 34450) and the analog readout of the microcontroller powered by energy harvesting coming from a smart phone working as reader.

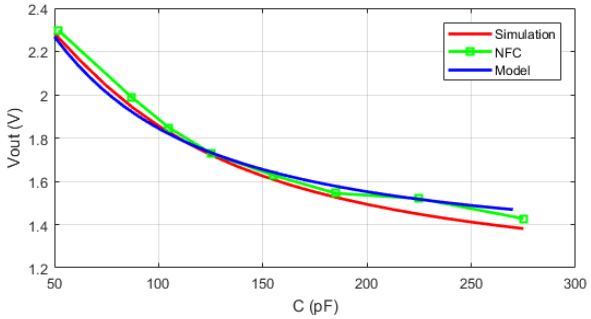

Fig. 7. Output voltage of the measurement system as a function of the sensor capacitance C. Comparison between the model proposed (11), the simulation, and the NFC read using a smartphone.

Performing a sensitivity analysis from the slope of the voltage as a function of the capacitance, the average error obtained from the 10-bits ADC of the microcontroller shown in Fig. 8 is under 2%, considering the capacitance range (55-270 pF) of the capacitor sensor proposed in this work.

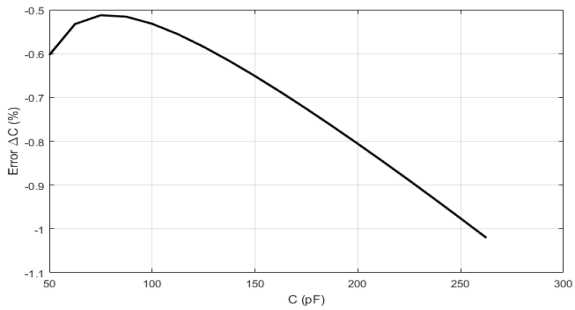

Fig. 8. Estimated error in the measurement of the capacitance from the analysis of sensitivity.

Fig. 9 shows the prototype manufactured on a FR4 PCB that consists of a NFC antenna, the chipset with a connector that gives access to the microcontroller in order to program it, and the interdigital capacitor which will be sunk into the soil.

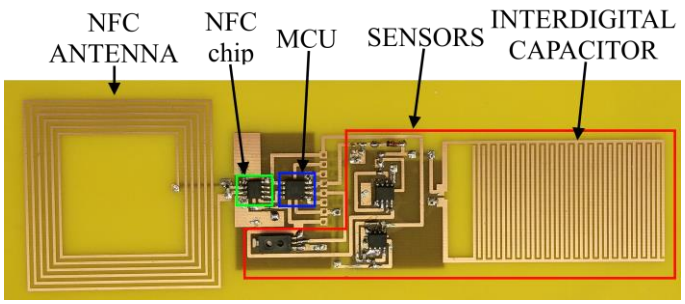

Fig.9. Designed PCB prototype with the antenna, the IDC and the chipset.

IV. Measurements

Any NFC enabled device can be used as a reader. Several smartphones have been tested (Xiaomi Mi Note 2, Sony Xperia Z1 and Huawei G8) reaching the threshold of the magnetic field to feed the tag by energy harvesting. Fig. 10(a) shows the energy harvested when it is illuminated with a smartphone, and Fig. 10(b) shows the data communication between the microcontroller, the tag and the sensors using the I^2C protocol. The tag is enabled to perform measurement using the four sink current modes of the NFC IC with the smart phone tested.

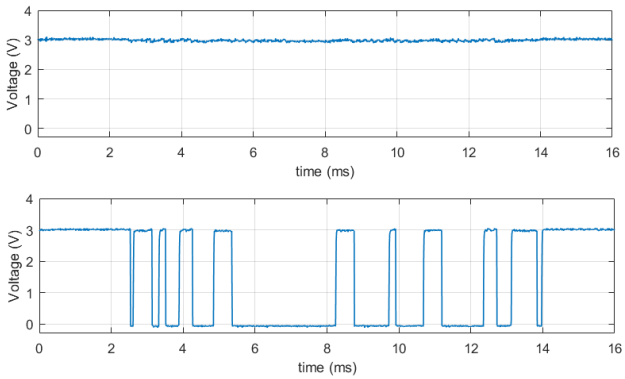

Fig. 10. Measurement of the energy harvesting output (a) and the data of SDA line from the I^2C bus (b) when the tag is powered by the NFC reader.

In order to ensure a constant DC voltage delivered by the NFC IC, the average magnetic field strength received by the tag must be above a certain threshold. The coupling of the antennas varies between different devices depending on the antenna shape and the surrounding materials. Thus, a measure of the maximum distance between the tag and the sensor has been experimentally measured with two commercial smartphones. The results presented on Fig. 11 shown differences in the read range. One of the devices has a maximum distance of about 8 mm whereas the second one almost reaches 20 mm. In both cases the rectified voltage goes to zero when the magnetic field strength is below 1 A/m. The threshold magnetic field depends on the efficiency of the internal rectifier of the NFC IC used. Therefore, the output power of the reader, the antenna's design and its integration within the mobile case depends on the model and consequently these factors have a great impact in the read range.

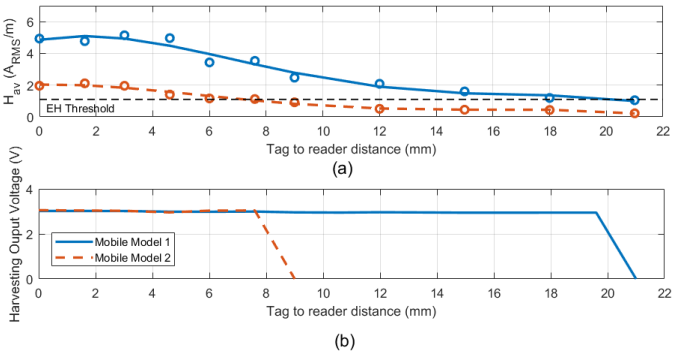

Fig.11. Average magnetic field received by the tag (a) and the rectified voltage (b) as function of the distance between the tag and the reader.

An application that runs in Android smartphone (shown in Fig. 12) has been developed as proof of concept. Beyond the sensed data, the system allows to send more information to the reader, such as a link to a website, or it can make use of the user identifier (UID) of each tag to give additional information of that specific product.

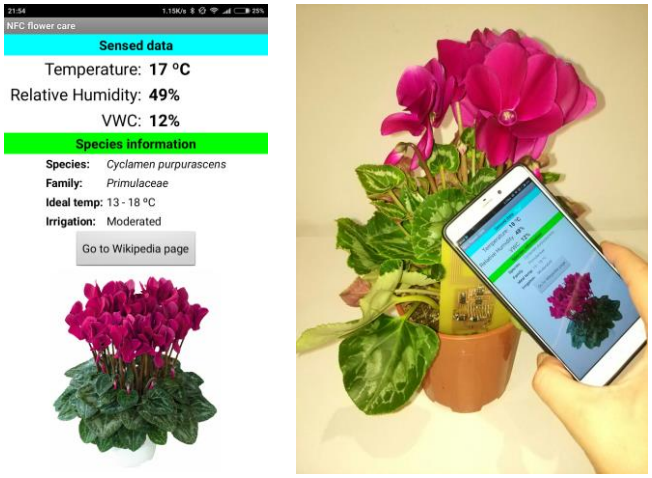

(a) (b)

Fig.12. Image of the developed app graphic interface which uses the tag UID to retrieve the information of the plant (a) and the flower pot with the device on it being powered and read by the smartphone (b).

To check the sensor operation an experimental setup and a calibration procedure is proposed. A typical soil used in greenhouses is chosen to perform the experiments. Different samples of soil are used with different volumetric water content, ranging from dry to water saturation. The interdigital capacitor is connected to a vector network analyser (VNA) that is used to measure the capacitance at 1 MHz. Fig. 13 shows the measurements of the capacitance as a function of the volumetric water content (blue squares) altogether with the two-point α-mixing model (12) (blue line). A capacitance of 65 pF is obtained when the soil is dried, which is considerably higher than when the sensor is on air (around 55 pF). It also shows the soil permittivity obtained from the relationship between the capacitance and the permittivity given by (7).

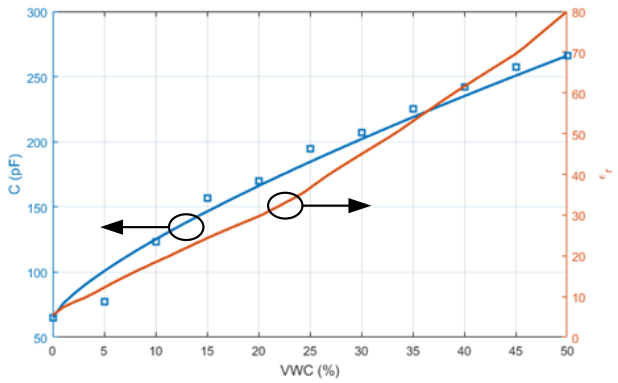

Fig.13. Measured capacitance (blue squares), model (12) (blue line) and relative permitivity (orange line) as a function of the volumetric water content.

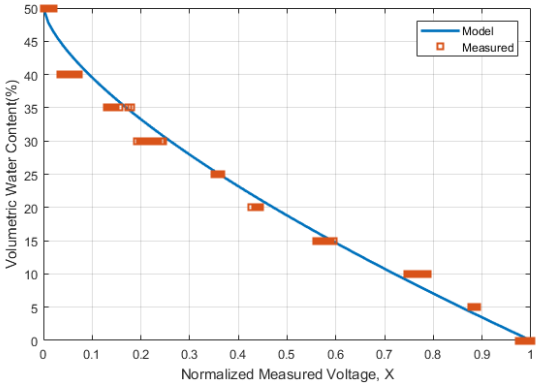

Fig.14. Comparison of measured (□) and modelled (13) volumetric water content as a function of the normalized voltage, X.

In order to achieve high accuracy, the sensor must be calibrated because the relation between the capacitance and the volumetric water content depends on the soil composition [28]. In addition, the capacitance as it is shown in Fig.4 depends on the coating thickness and the coating material. Therefore, a calibration system is needed. In order to calibrate the sensor, the two-point α-mixing model is fitted [28]. The volumetric water content is modelled as:

$$VWC(\%) = \frac{X^{\alpha} - X_{sat}^{\alpha}}{X_{dry}^{\alpha} - X_{sat}^{\alpha}}\phi \qquad (12)$$

Where X is a variable that depends on the sensor measurement, α is a fitting parameter that depends on the sensor and ϕ is the porosity of the medium. The sub-indexes dry and sat correspond to the sensor output values when soil is dry and when it is water-saturated, respectively.

The fitting parameter α depends on the sensor and is obtained from the slope in logarithmic scale:

$$\alpha = \frac{ln\left(1-\frac{VWC}{\phi}\right)}{\ln(X)} \qquad (13)$$

Taking into account that the proposed circuit has an output voltage proportional to the VWC, it is possible to define X as the normalized measured voltage (Fig. 6):

$$X = \frac{V_{out} - V_{out,min}}{V_{out,max} - V_{out,min}} \qquad (14)$$

Where $V_{out,min}$ and $V_{out,max}$ are the minimum (on water) and maximum (on air) measured output voltages, respectively. Therefore, using this normalized variable X, X_{dry}=1 and X_{sat}=0. It is straightforward to calculate α and ϕ from a linear fitting in logarithmic scale.

The values obtained for α and ϕ are 0.33 and 50%, respectively. Fig. 14 shows the results of the volumetric water content as a function of the normalized voltage, comparing the model with the measured values.

In order to analyze the behavior of the sensor during the irrigation process a setup with 11 different pots, containing a blended mixture with different quantities of water, from dried soil to 50% of VWC in steps of 5% have been set. Thus, a heterogeneous distribution of the water along the soil is assured. The sensor has been on each pot enough time to take 50 samples. The result is shown in Fig. 15, where it can be seen the stability of the measured VWC until it reaches the 45%, where the sensor is saturated. In order to simulate the drying process, the same procedure has been done from 50% to 0%. VWC.

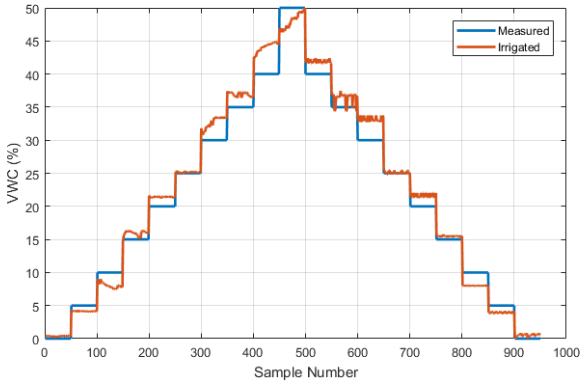

Fig.15. Computed VWC compared to the irrigated water.

Fig. 16 shows the behavior of the sensor after an irrigation of 150 ml of water on a 1-liter pot which initially had present about 13% of VWC. The figure compares the measurements of the presented sensor with a commercial sensor (Decagon EC-5). As it is shown, the commercial sensor has a smother response whereas the NFC sensor has a faster reaction. The fast initial increase of VWC (at 5 min) is due to the presence of the water on the sensor surface. The two sensors give the same final

steady state value after all the water has been diffused in the recipient.

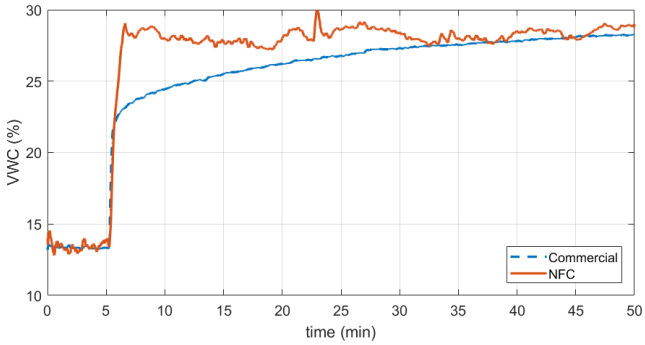

Fig.16. Measurement of VWC after irrigation of the proposed NFC sensor and a commercial soil moisture sensor.

V. Conclusions

This work has presented a low-cost, battery-less, NFC-powered device that is capable to measure volumetric water content (soil moisture), temperature and relative humidity and show it on a smartphone application or upload it to the cloud to be shared or stored. The proposed solution combines commercial sensors for temperature and relative humidity along with a specific method to measure the soil's volumetric water content, based on a capacitive measure which has been selected between the different possible methods found in the literature considering the NFC constraints. A printed interdigital capacitor using conventional PCB technology has been designed, fabricated, and measured for this purpose. The effect of an insulator layer for corrosion protection has been analyzed. An accurate capacitance measurement method based on a low-power oscillator and a diode-based detector is employed. A procedure for the calibration of the sensor has been presented based on a simple expression whose coefficients can be experimentally obtained.

The work has shown that the magnetic field generated by a standard smartphone is strong as well as stable enough to supply the energy for the designed system.

References

[1] Near field communications forum. [Online]. Available: http://nfc-forum.org
[2] ST Microelectronics, "Dynamic NFC/RFID tag IC with 4-Kbit EEPROM, energy harvesting, I²C bus and ISO 15693 RF interface," , M24LR04E-R datasheet, Jul.2017,
[3] AMS, Datasheet: AS3956 "NFC Sensor Interface Tag IC," AS3956 datasheet, Oct.2017.
[4] NXP Semiconductors, Datasheet: "NTAG I2C - Energy harvesting NFC Forum Type 2 Tag with field detection pin and I2C interface," NT3H1101/NT3H1201 datasheet, Jul.2015.
[5] J. J. Wikner, J. Zötterman, A. Jalili, and S. Farnebo, "Aiming for the cloud - a study of implanted battery-free temperature sensors using NFC," in *2016 International Symposium on Integrated Circuits (ISIC)*, 2016, pp. 1–4.
[6] R. Rahimi, U. Brener, M. Ochoa, and B. Ziaie, "Flexible and transparent pH monitoring system with NFC communication for wound monitoring applications," in *2017 IEEE 30th International Conference on Micro Electro Mechanical Systems (MEMS)*, 2017, pp. 125–128.
[7] S. G. Reynolds, "The gravimetric method of soil moisture determination Part IA study of equipment, and methodological problems," *Journal of Hydrology*, vol.11, no.3, pp.258-273, 1970.
[8] Y. Kim, R. G. Evans and W. M. Iversen, "Remote Sensing and Control of an Irrigation System Using a Distributed Wireless Sensor Network," in IEEE Transactions on Instrumentation and Measurement, vol. 57, no. 7, pp. 1379-1387, July 2008.
[9] J. Gutiérrez, J. F. Villa-Medina, A. Nieto-Garibay and M. Á. Porta-Gándara, "Automated Irrigation System Using a Wireless Sensor Network and GPRS Module," in IEEE Transactions on Instrumentation and Measurement, vol. 63, no. 1, pp. 166-176, Jan. 2014.
[10] D.A. Robinson, S.B. Jones, J.A. Wraith, D. Or, S.P., Firedmena, "A review of advances in dielectric and electrical conductivity measurements in soils using time domain reflectometry," *Vadose Zone Journal*, vol.2, no. 4, pp.444–475, 2003
[11] D. F. Sinclair, J. Williams, "Components of variance involved in estimating soil water content and water content change using a neutron moisture meter," *Soil Research*, vol.17, no.2, pp.237-247, 1979.
[12] S. R.Evett, J.A. Tolk, T.A. Howell, "A depth control stand for improved accuracy with the neutron probe," *Vadose Zone Journal*, vol.2, no.4, pp.642-649, 2003.
[13] G.S. Campbell, G.W. Gee, "Water potential: miscellaneous methods. Methods of Soil Analysis: Part 1", *Physical and Mineralogical Methods*, methodsofsoilan1, 619-633, 1986.
[14] S.B. Jones, J.M. Wraith, D. Or, "Time domain reflectometry measurement principles and applications" *Hydrological processes*, vol.16, no.1, pp.141-153, 2002.
[15] A. Cataldo, E. De Benedetto, G. Cannazza, E. Piuzzi and E. Pittella, "TDR-Based Measurements of Water Content in Construction Materials for In-the-Field Use and Calibration," *IEEE Transactions on Instrumentation and Measurement*, vol. PP, no. 99, pp. 1-8, 2017.
[16] Campbell Scientific, "Time-Domain Reflectometry System," TDR200, SDM8X50, CS600-series datasheet, July 2016,
[17] K. Y. You et al., "Precise Moisture Monitoring for Various Soil Types Using Handheld Microwave-Sensor Meter," *IEEE Sensors Journal*, vol. 13, no. 7, pp. 2563-2570, July 2013.
[18] K. Xu, Q. Sheng, X. Zhang, P. Li and S. Chen, "Design and Calibration of the Unilateral Sensitive Soil Moisture Sensor," *IEEE Sensors Journal*, vol. 15, no. 8, pp. 4587-4594, Aug. 2015.
[19] D. Wobschall, "A Frequency Shift Dielectric Soil Moisture Sensor," *IEEE Transactions on Geoscience Electronics*, vol. 16, no. 2, pp. 112-118, April 1978.
[20] J. B. Ong, Z. You, J. Mills-Beale, E. L. Tan, B. D. Pereles and K. G. Ong, "A Wireless, Passive Embedded Sensor for Real-Time Monitoring of Water Content in Civil Engineering Materials," *IEEE Sensors Journal*, vol. 8, no. 12, pp. 2053-2058, Dec. 2008.
[21] T.J. Dean, J.P. Bell, A.J.B. Baty, "Soil moisture measurement by an improved capacitance technique, Part I. Sensor design and performance," *Journal of Hydrology*, vol.93, no.1-2, 67-78, 1987.
[22] Atmel Corp., "Atmel tiny 85 8-bit AVR Microcontroller with 2/4/8K Bytes In-System Programmable Flash," Tiny 85 datasheet, 2013
[23] Texas Instruments, Datasheet: LM75A "Digital Temperature Sensor and Thermal Watchdog With Two-Wire Interface," LM75A datasheet, Dec.2014.
[24] Honeywell, Datasheet: HIH-5030/5031 Series datasheet, 2010.
[25] S.Gevorgian, T. Martinsson, P. Linner, and E. Kolberg ''CAD Models for Multi-Layered Substrate Interdigital Capacitors,'' *IEEE Trans. Microwave Theory Tech.*, vol. 44, no.6, pp. 162–164, 1996.
[26] J. Svacina, "Analysis of multilayer microstrip lines by a conformal mapping method," *IEEE Transactions on Microwave Theory and Techniques*, vol. 40, no. 4, pp. 769-772, Apr 1992.
[27] J.W.Kim, " Development of interdigitated capacitor sensors for direct and wireless measurements of the dielectric properties of liquids", PhD. Dissertation, The University of Texas at Austin, 2008.
[28] T. Sakaki, A., Limsuwat, T. H. Illangasekare, "A simple method for calibrating dielectric soil moisture sensors: Laboratory validation in sands." *Vadose Zone Journal*, vol.10, no.2, pp.526-531, 2011.

Martí Boada received the B.Sc. in telecommunications engineering from Universitat Rovira I Virgili (URV), Tarragona, Spain, in 2012 and the M.Sc. in telecommunications engineering and management from Universitat Politècnica de Catalunya (UPC), Barcelona, Spain, in 2014. Since 2017 he is pursuing the Ph.D. degree at the Department of Electronic Engineering of the URV. His research activities are focused on microwave devices and systems, with an emphasis on RFID, NFC and wireless sensors..

Antonio Lázaro (M'07,SM'16) was born in Lleida, Spain, in 1971. He received the M.S. and Ph.D. degrees in telecommunication engineering from the Universitat Politècnica de Catalunya (UPC), Barcelona, Spain, in 1994 and 1998, respectively. He then joined the faculty of UPC, where he currently teaches a course on microwave circuits and antennas. Since July 2004, he is a Full-Time Professor at the Department of Electronic Engineering, Universitat Rovira i Virgili (URV), Tarragona, Spain. His research interests are microwave device modeling, on-wafer noise measurements, monolithic microwave integrated circuits (MMICs), low phase noise oscillators, MEMS, RFID, UWB and microwave systems.

Ramon Villarino received the Telecommunications Technical Engineering degree from the Ramon Llull University (URL), Barcelona, Spain in 1994, the Senior Telecommunications Engineering degree from the Polytechnic University of Catalonia (UPC), Barcelona, Spain in 2000 and the PhD from the UPC in 2004. During 2005-2006, he was a Research Associate at the Technological Telecommunications Center of Catalonia (CTTC), Barcelona, Spain. He worked at the Autonomous University of Catalonia (UAB) from 2006 to 2008 as a Researcher and Assistant Professor. Since January 2009 he is a Full-Time Professor at Universitat Rovira i Virgili (URV). His research activities are oriented to radiometry, microwave devices and systems, based on UWB, RFIDs and frequency selective structures using MetaMaterials (MM).

David Girbau (M'04, SM'13) received the BS in Telecommunication Engineering, MS in Electronics Engineering and PhD in Telecommunication from Universitat Politècnica de Catalunya (UPC), Barcelona, Spain, in 1998, 2002 and 2006, respectively. From February 2001 to September 2007 he was a Research Assistant with the UPC. From September 2005 to September 2007 he was a Part-Time Assistant Professor with the Universitat Autònoma de Barcelona (UAB). Since October 2007 he is a Full-Time Professor at Universitat Rovira i Virgili (URV). His research interests include microwave devices and systems, with emphasis on UWB, RFIDs, RF-MEMS and wireless sensors.